Doubly Selective Channel Estimation for FBMC and OFDM Systems Based on MIR Correlation

Ying Wang, *Graduate Student Member, IEEE*, Qiang Guo, Jianhong Xiang, *Member, IEEE*, and Yu Zhong

***Abstract*—Filter Bank Multi-Carrier (FBMC) modulation based on offset quadrature amplitude modulation has superior spectral properties than Orthogonal Frequency Division Multiplexing (OFDM). However, many existing OFDM channel estimation schemes cannot be compatible with FBMC due to inherent interference. In this letter, we propose a channel estimation method based on Measured Impulse Response (MIR) correlation, which enables compatibility with arbitrary linear modulation techniques. To ensure estimation accuracy, we combine the MIR correlation values and the orthogonal projection theorem to derive extrapolation factors instead of linear extrapolation. Additionally, for FBMC, we mitigate the interference at pilot positions by adding guard symbols. Note that although the correlation values are calculated based on the measured values, it still provides a high estimation accuracy. Simulation results show that our scheme is compatible with OFDM and FBMC, and the estimation accuracy can reach –30dB.**

***Index Terms*—OFDM, FBMC, channel estimation, measured impulse response (MIR), orthogonal projection theorem.**

I. Introduction

MULTI-CARRIER systems enable parallel data transmission with high rates. Orthogonal Frequency Division Multiplexing (OFDM) is the major technique in current wireless broadband systems and will continue to play a role in 5G wireless systems. However, Filter Bank Multi-Carrier (FBMC) modulation based on Offset Quadrature Amplitude Modulation (OQAM) has been widely studied as an alternative to OFDM due to its superior spectral properties [1].

In doubly selective channels, OFDM is affected by channel-induced interference, while FBMC is affected by inherent interference [2] and channel-induced interference. Thus, many OFDM techniques are not compatible with FBMC. To estimate the doubly selective channel, Fu et al. [3] proposed a deep learning based joint pilot design and channel estimation scheme in closed-loop OFDM. However, the scheme is difficult to apply to open-loop OFDM. In open-loop OFDM, the classical estimation scheme is realized by combining the base extension model and distributed compressed sensing [4]. However, the high complexity of the reconstruction algorithm leads to increased latency. For FBMC, Ren et al. [5], [6] proposed joint channel estimation and preamble channel estimation schemes. Chen et al. [7] proposed channel estimation and pilot frequency optimization for interference utilization. Kong et al. [8], [9] proposed interference cancelation with frame repetition and channel estimation scheme with symbol repetition. Liu et al. [10] proposed a preamble-based channel estimation scheme for FBMC with delayed diversity. All these schemes significantly improve the accuracy of channel estimation for FBMC system. It is worth noting that the above channel estimation techniques are not compatible with both OFDM and FBMC systems. Thus, we investigate the channel estimation scheme that is not only compatible with OFDM and FBMC systems, but also applicable to arbitrary linear modulation techniques. Our main contributions can be summarized below:

1) This letter proposes a doubly selective channel estimation scheme based on measured impulse response correlation, which does not require a clustered pilot or base extension model. Specifically, the estimated channel is calculated by combining the measured impulse response correlation value and the pilot position channel correlation value. The scheme is applicable to arbitrary linear modulations, with OFDM and FBMC being typical cases.
2) We derive the Non-Interference Removal (NIR) and Interference Removal (IR) extrapolation factors. Specifically, using the measured impulse response correlation values and the orthogonal projection theorem, we provide Lemma 1 for calculating the NIR extrapolation factor. To reduce the interference of received symbols (including the pilots), we adopt differential interference cancelation and calculate the IR extrapolation factor.
3) We provide measurements and adopt the 3GPP “Extended Vehicular A” channel model to verify the reliability of the estimation scheme. The results show that our scheme works robustly in doubly selective channels and the measured values describe the real values with a tolerance of 7%-12%.[1]

Notation: diag$\{\cdot\}$ denotes the diagonal elements of a matrix. $(\cdot)^{-1}$, $(\cdot)^{*}$, $(\cdot)^{T}$ and $(\cdot)^{H}$ denote inverse, conjugate, transpose, and conjugate transpose operations, respectively. vec$\cdot$ denotes column-wise vectorization. $\circ$ and $\otimes$ denote the Hadamard product and the Kronecker product, respectively.

Received 1 November 2024; revised 11 December 2024; accepted 1 January 2025. Date of publication 3 January 2025; date of current version 10 March 2025. This work was supported in part by the Fundamental Research Funds for the Central Universities, China, under Grant 3072022CF0801, and in part by the Sichuan Provincial Key Laboratory of Agile Intelligent Computing Project Fund, China. The associate editor coordinating the review of this article and approving it for publication was L. Sboui. *(Corresponding author: Jianhong Xiang.)*

Ying Wang, Qiang Guo, and Jianhong Xiang are with the College of Information and Communication Engineering, Harbin Engineering University, Harbin 150001, China (e-mail: wangyingstu@163.com; guoqiang@hrbeu.edu.cn; xiangjianhong@hrbeu.edu.cn).

Yu Zhong is with the 10th Research Institute, China Electronics Technology Group Corporation, Chengdu 610036, China (e-mail: jade.zhong@hotmail.com).

Digital Object Identifier 10.1109/LWC.2025.3525592

[1]The detailed code tutorial for this letter can be downloaded at **https://github.com/WangYeeng/CE_for_FBMC_and_OFDM_master**.

II. System Model

In multicarrier systems, the transmitted information is mapped in 2D time-frequency grids, which are mainly characterized by base pulses. Mathematically, the time-domain transmitted signal $s(t)$ of a multicarrier system can be expressed as

$$s(t) = \sum_{k=1}^{K}\sum_{l=1}^{L} x_{l,k} \underbrace{p(t-kT)\exp(j2\pi lF(t-kT))}_{g_{l,k}(t)}, \quad (1)$$

where $x_{l,k}$ denotes the transmitted symbols at time position k and frequency position l. $p(t)$ denotes the prototype filter. $g_{l,k}(t)$ denotes the base pulse. T denotes the symbol period and $F = \frac{1}{T}$ the subcarrier spacing. After wireless channel transmission, we can obtain the received signal $r(t)$, denoted as

$$r(t) = \int_{\mathbb{R}} s(\tau)h(t,\tau)\mathrm{d}\tau + \mathrm{n}(t), \quad (2)$$

where $h(t,\tau)$ denotes the time variant multipath channel [11] and $\mathrm{n}(t)$ the noise. The received symbol $y_{l,k}$ is obtained by performing the inner product of the received signal with the base pulse, written as

$$y_{l,k} = \int_{\mathbb{R}} r(t)g^*_{l,k}(t)\mathrm{d}t. \quad (3)$$

Note that Eq. (3) corresponds to matched filtering with maximized output Signal-to-Noise Ratio (SNR). Now, we switch the continuous time domain to the discrete time domain for practical applications. We adopt the rate f_s to sample the base pulse and represent the sampled values with the vector $\mathbf{g}_{l,k} \in \mathbb{C}^{N\times 1}$. Then, all the base pulse vectors are integrated into the transmitted matrix $\mathbf{G} = [\mathbf{g}_{1,1},\ldots,\mathbf{g}_{L,K}] \in \mathbb{C}^{N\times LK}$. Thereby, the matrix algebra model of the multicarrier system reads

$$\mathbf{y} = \mathbf{G}^H\mathbf{H}\mathbf{G}\mathbf{x} + \mathbf{n} = \boldsymbol{\mathcal{H}}\mathbf{x} + \mathbf{n}, \quad (4)$$

where $\mathbf{x} = [x_{1,1},\ldots x_{L,K}]^T \in \mathbb{C}^{LK\times 1}$ denotes the transmitted symbol, typically selected from the Quadrature Amplitude Modulation (QAM) symbol alphabet. $\mathbf{H} \in \mathbb{C}^{N\times N}$ denotes the time variant convolution matrix [12]. $\mathbf{y} = [y_{1,1},\ldots y_{L,K}]^T \in \mathbb{C}^{LK\times 1}$ denotes the received symbol. $\mathbf{n} \sim \mathcal{CN}(\mathbf{0}, P_{\mathrm{n}}\mathbf{G}^H\mathbf{G})$ denotes Gaussian noise with power P_{n}.

In CP-OFDM, the transmitted prototype filter $p_{TX}(t)$ is a rectangular function, and the received prototype filter $p_{RX}(t)$ is a rectangular function with CP removed. We denote such difference implicitly in $\mathcal{H} \in \mathbb{C}^{LK\times LK}$, and then the orthogonality of CP-OFDM is described as $\mathbf{G}^H\mathbf{G} = \mathbf{I}_{LK}$. Thus, in a flat channel, the CP-OFDM model can be simplified as

$$y_{l,k} = h_{l,k}x_{l,k} + \mathrm{n}_{l,k}, \quad st.\ h_{l,k} = [\mathrm{diag}\{\boldsymbol{\mathcal{H}}\}]_{l+kL}, \quad (5)$$

where $h_{l,k}$ denotes the one-tap channel at subcarrier position l and time position k, and $\mathrm{n}_{l,k}$ the corresponding noise. In FBMC, the receiver can use the same prototype filter as the transmitter. However, at the transmitter of FBMC, the real and imaginary parts of a complex-valued QAM symbol with period T are regarded as two consecutive real-valued OQAM symbols with period $\frac{T}{2}$. Thus, complex orthogonality is replaced by real orthogonality, leading to interference. Note that multiplying each OQAM symbol by the phase shift factor $\exp(\frac{j\pi(l+k)}{2})$ can concentrate the interference all in the imaginary domain. The orthogonality of FBMC can be described as $\Re\{\mathbf{G}^H\mathbf{G}\} = \mathbf{I}_{LK}$. Thus, in a flat channel, the FBMC model can be simplified as

$$\begin{aligned} y_{l,k} &= h_{l,k}\big(x_{l,k} + j\Im\{\mathbf{q}_{l,k}\}\mathbf{x}\big) + \mathrm{n}_{l,k} \\ st.\ h_{l,k} &= [\mathrm{diag}\{\boldsymbol{\mathcal{H}}\}]_{l+kL}, \end{aligned} \quad (6)$$

where $\mathbf{q}_{l,k} = [\mathbf{G}^H\mathbf{G}]_{l+kL}$ and $j\Im\{\mathbf{q}_{l,k}\}\mathbf{x}$ denotes the imaginary interference term. Considering the imaginary interference reasonably, we can design the channel estimation scheme applicable to OFDM and FBMC. Generally, $h_{l,k}$ is easier to estimate than $\mathcal{H}$. However, in doubly selective channels, OFDM is affected by channel-induced interference, while FBMC is affected by both inherent and channel-induced interference. All interferences are described as off-diagonal elements of $\mathcal{H}$. Because Eqs. (5) and (6) cannot accurately describe all interferences, the validity of the modeling is reduced. In this case, we rely on the model of Eq. (4). Thus, in harsh transmission environments, it is more efficient for us to estimate $\mathcal{H} \in \mathbb{C}^{LK\times LK}$ directly instead of $h_{l,k}$

III. Channel Estimation

In open-loop OFDM, equally spaced pilot sequences have been theoretically proven to be the optimal choice for Least Squares (LS) channel estimation [13]. Also, the resource overhead can be minimized [14]. Therefore, considering the compatibility of arbitrary linear modulation schemes, we adopt a scattered LTE diamond-shaped pilot structure [15] and use LS to estimate the Channel of Pilot Position (CoPP). FBMC does not employ CP. Thus, we can mitigate imaginary interference using guard symbols, which does not incur additional resource overhead compared to CP-OFDM. If $|\mathcal{P}|$, $|\mathcal{D}|$ and $|\mathcal{G}|$ denote the number of pilot, data and guard symbols respectively, then $\mathbf{x}_{\mathcal{P}} \in \mathbb{C}^{|\mathcal{P}|\times 1}$, $\mathbf{x}_{\mathcal{D}} \in \mathbb{C}^{|\mathcal{D}|\times 1}$ and $\mathbf{x}_{\mathcal{G}} \in \mathbb{C}^{|\mathcal{G}|\times 1}$ denote the pilot, data and guard symbols respectively. The LS estimated value of CoPP can be calculated as

$$\hat{h}_{\mathcal{P}_i} = \sqrt{\rho}\,y_{\mathcal{P}_i}/x_{\mathcal{P}_i}\ , \quad (7)$$

where ρ denotes the pilot-data power offset. $\mathcal{P}_i$ denotes the ith pilot position. We stack all the estimated CoPP in the vector $\hat{\mathbf{h}}_{\mathcal{P}} = [\hat{h}_{\mathcal{P}_1},\ldots,\hat{h}_{\mathcal{P}_{|\mathcal{P}|}}]^T \in \mathbb{C}^{|\mathcal{P}|\times 1}$, and obtain the channel information at data positions by extrapolation, denoted as

$$\hat{h}_{l,k} = \boldsymbol{\Upsilon}^H_{l,k}\hat{\mathbf{h}}_{\mathcal{P}}, \quad (8)$$

where $\boldsymbol{\Upsilon}_{l,k} \in \mathbb{C}^{|\mathcal{P}|\times 1}$ denotes the extrapolation factor of subcarrier position l and time position k. In flat channels, we can use minimum mean square error or linear extrapolation, etc. However, for doubly selective channels, the extrapolation of Eq. (8) is no longer valid. We need to directly estimate $\mathcal{H} \in \mathbb{C}^{LK\times LK}$ using the estimated CoPP, denoted as

$$\hat{\boldsymbol{\mathcal{H}}} = \sum\nolimits_{i=1}^{|\mathcal{P}|} \boldsymbol{\Lambda}_i\hat{h}_{\mathcal{P}_i}, \quad st.\ \ [\boldsymbol{\Lambda}_i]_{\ell 1,\ell 2} = \Big[\boldsymbol{\Upsilon}^H_{l1,k1,l2,k2}\Big]_i, \quad (9)$$

where $\ell 1 = l_1 + k_1L \in [1, LK]$ and $\ell 2 = l_2 + k_2L \in [1, LK]$. Like $\boldsymbol{\Upsilon}_{l,k}$, $\boldsymbol{\Upsilon}^H_{l1,k1,l2,k2} \in \mathbb{C}^{|\mathcal{P}|\times 1}$ is the extrapolation factor which can extrapolate interference information. When $l = l_1 = l_2$ and $k = k_1 = k_2$, $\boldsymbol{\Upsilon}_{l1,k1,l2,k2} = \boldsymbol{\Upsilon}_{l,k}$. Thus, Eq. (9)

can also be used to directly estimate the one-tap channel, i.e., $\hat{h}_{l,k} = [\mathrm{diag}\{\hat{\boldsymbol{\mathcal{H}}}\}]_\ell$. The extrapolation factor effects the channel estimation accuracy significantly. However, directly obtaining $\boldsymbol{\Upsilon}^H_{l1,k1,l2,k2}$ usually faces significant challenges due to channel-induced interference. The reason is that we lack a priori information to support high-accuracy extrapolation. Fortunately, using the orthogonal projection theorem [16] and combining it with the Measured Impulse Response (MIR), we can calculate the extrapolation matrix $\boldsymbol{\Lambda} \in \mathbb{C}^{LK\times LK\times|\mathcal{P}|}$.

Lemma 1: In the system model $\mathbf{y} = \mathcal{H}\mathbf{x} + \mathbf{n}$, if the correlation matrix $\mathbf{R}_\mathbf{H} \in \mathbb{C}^{N^2\times N^2}$ of MIR-($\mathbf{H}$) is available, then there exists a matrix $\boldsymbol{\Lambda} \in \mathbb{C}^{LK\times LK\times|\mathcal{P}|}$ such that $\hat{\mathcal{H}}$ satisfies the orthogonal projection theorem and can be calculated as

$$f : \left\{\mathbf{R}_{\boldsymbol{\mathcal{H}},\mathbf{h}_\mathcal{P}}\left(\mathbf{R}_{\mathbf{h}_\mathcal{P}}\right)^{-1}, L^2K^2 \times |\mathcal{P}|\right\} \rightarrow f : \{\boldsymbol{\Lambda}, LK \times LK \times |\mathcal{P}|\}. \tag{10}$$

Proof: The proof is provided in the Appendix, where $\mathbf{R}_{\mathcal{H},\mathbf{h}_\mathcal{P}} \in \mathbb{C}^{L^2K^2\times|\mathcal{P}|}$ denotes the inter-correlation matrix between $\mathcal{H}$ and CoPP-($\mathbf{h}_\mathcal{P} \in \mathbb{C}^{|\mathcal{P}|\times 1}$), and $\mathbf{R}_{\mathbf{h}_\mathcal{P}} \in \mathbb{C}^{|\mathcal{P}|\times|\mathcal{P}|}$ denotes the autocorrelation matrix of $\mathbf{h}_\mathcal{P}$. $f : \{\cdot\}$ denotes the mapping relationship of matrix dimensions, with column-major priority. To adopt Lemma 1, we need to calculate $\mathbf{R}_{\boldsymbol{\mathcal{H}},\mathbf{h}_\mathcal{P}}$ and $\mathbf{R}_{\mathbf{h}_\mathcal{P}}$ efficiently. Specifically, according to $\mathbf{R}_\mathbf{H} \in \mathbb{C}^{N^2\times N^2}$, we first calculate $\mathbf{R}_{\boldsymbol{\mathcal{H}},\mathbf{h}_\mathcal{P}} \in \mathbb{C}^{L^2K^2\times|\mathcal{P}|}$, denoted as

$$f : \{\mathbf{R}_\mathbf{H}\left(\mathbf{g}^T_{\mathcal{P}_i} \otimes \mathbf{g}^H_{\mathcal{P}_i}\right)^H, N^2 \times 1\} \rightarrow f : \{\mathbf{r}_{\mathbf{h}_{\mathcal{P}_i}}, N \times N\}, \tag{11}$$

$$f : \{\mathbf{G}^H\mathbf{r}_{h_{\mathcal{P}_i}}\mathbf{G}, LK \times LK\} \rightarrow f : \{\mathbf{R}_{\boldsymbol{\mathcal{H}},\mathbf{h}_{\mathcal{P}_i}}, L^2K^2 \times |\mathcal{P}_i|\}, \tag{12}$$

where $\mathbf{R}_\mathbf{H} = \mathbb{E}\{\mathrm{vec}\{\mathbf{H}\}\mathrm{vec}\{\mathbf{H}\}^H\}$. $\mathbf{g}_{\mathcal{P}_i} \in \mathbb{C}^{N\times 1}$ denotes the base pulse of the ith pilot. In practice, $\mathbf{R}_\mathbf{H}$ is unknown. However, the indoor measurement methods provided in [17], [18] are available. The reason is that the measured value of $\mathbf{R}_\mathbf{H}$ behaves similarly to the actual value in terms of attenuation and correlation in time/frequency. Note that the effectiveness depends on the measurement environment. Traveling Eqs. (11)-(12) over all pilot positions, we obtain $\mathbf{R}_{\boldsymbol{\mathcal{H}},\mathbf{h}_\mathcal{P}} \in \mathbb{C}^{L^2K^2\times|\mathcal{P}|}$. Secondly, based on $\mathbf{R}_\mathbf{H} \in \mathbb{C}^{N^2\times N^2}$, we can calculate $\mathbf{R}_{\mathbf{h}_\mathcal{P}} \in \mathbb{C}^{|\mathcal{P}|\times|\mathcal{P}|}$, denoted as

$$\begin{aligned}&[\mathbf{R}_{\mathbf{h}_\mathcal{P}}]_{\mathcal{P}_i,\mathcal{P}_i}\\ &= \left|\sum_{\ell=1}^{LK}\sum_{n=1}^{N}\left[\left(\mathbf{G}^T(\boldsymbol{\xi}\mathbf{R}_\mathbf{H}\boldsymbol{\xi}^H)\right)\circ\mathbf{G}^H\right]_{:,n}\right| + \frac{P_\mathrm{n}}{\rho}\mathbf{g}^H_{\mathcal{P}_i}\mathbf{g}_{\mathcal{P}_i}\\ &st.\ \boldsymbol{\xi} = \frac{1}{\sqrt{\rho}}\left(\mathbf{I}_N \otimes \mathbf{g}^H_{\mathcal{P}_i}\right)\end{aligned} \tag{13}$$

where $\boldsymbol{\xi} \in \mathbb{C}^{N\times N^2}$ denotes the sieve matrix for pilot positions. Traveling Eq. (13) over all pilot positions, we obtain $\mathbf{R}_{\mathbf{h}_\mathcal{P}} \in \mathbb{C}^{|\mathcal{P}|\times|\mathcal{P}|}$. Finally, by Lemma 1, we can calculate $\boldsymbol{\Lambda} \in \mathbb{C}^{LK\times LK\times|\mathcal{P}|}$. Note that Lemma 1 derives $\boldsymbol{\Lambda} \in \mathbb{C}^{LK\times LK\times|\mathcal{P}|}$ using the correlation matrix of MIR-($\mathbf{H}$) as prior information. Thus, extrapolation accuracy is dependent on the measurement environments.

So far, the extrapolation matrix we have calculated attempts to infer the interference (i.e., the off-diagonal elements of $\boldsymbol{\mathcal{H}}$) based on the measurement information, which is hardly satisfactory for doubly selective channels. The reason is that measurement information cannot fully and accurately describe the actual interference. Fortunately, received symbols can remove interference effects [15]. This means that we can estimate $\boldsymbol{\mathcal{H}}$ directly without inferring the interference case. The received symbol $\bar{\mathbf{y}} \in \mathbb{C}^{LK\times 1}$ with interference removed can be calculated as

$$\bar{\mathbf{y}} = \mathbf{y} - \left(\hat{\boldsymbol{\mathcal{H}}} - \mathrm{diag}\{\hat{\boldsymbol{\mathcal{H}}}\}\right)\boldsymbol{\mathcal{A}}\begin{bmatrix}\mathbf{x}_\mathcal{P}\\ \hat{\mathbf{x}}_\mathcal{D}\end{bmatrix}, \tag{14}$$

where $\boldsymbol{\mathcal{A}} \in \mathbb{C}^{LK\times(|\mathcal{P}|+|\mathcal{D}|)}$ denotes an auxiliary matrix that ensures the correct mapping of data and pilot positions. $\hat{\mathbf{x}}_\mathcal{D}$ denotes the detected data symbol (generally the ZF equalizer is sufficient). Note that $\hat{\boldsymbol{\mathcal{H}}}$ is estimated from the NIR extrapolation factor. To calculate the IR extrapolation factor, we need to recalculate the autocorrelation matrix $\bar{\mathbf{R}}_{\mathbf{h}_\mathcal{P}}$ for $\mathbf{h}_\mathcal{P}$:

$$\boldsymbol{\mathcal{R}}_{\mathbf{h}_{\mathcal{P}_i}} = \sum_{n=1}^{N}\left[\left(\mathbf{G}^H_\mathcal{P}\mathbf{r}_{\mathbf{h}_{\mathcal{P}_i}}\right)\circ\mathbf{G}^T_\mathcal{P}\right]_{:,n} \in \mathbb{C}^{|\mathcal{P}|\times|\mathcal{P}_i|}, \tag{15}$$

where $\mathbf{G}_\mathcal{P} \in \mathbb{C}^{N\times|\mathcal{P}|}$ denotes the transmitted matrix for pilots. Traveling Eq. (15) over all pilot positions, we can obtain $\boldsymbol{\mathcal{R}}_{\mathbf{h}_\mathcal{P}} \in \mathbb{C}^{|\mathcal{P}|\times|\mathcal{P}|}$. Thus, $\bar{\mathbf{R}}_{\mathbf{h}_\mathcal{P}}$ can be calculated as

$$\begin{aligned}&[\bar{\mathbf{R}}_{\mathbf{h}_\mathcal{P}}]_{\mathcal{P}_i,\mathcal{P}_i} = [\mathbf{R}_{\mathbf{h}_\mathcal{P}}]_{\mathcal{P}_i,\mathcal{P}_i}\\ &-\left(\left|\sum_{\ell=1}^{LK}\sum_{n=1}^{N}\left[\left(\mathbf{G}^T(\boldsymbol{\xi}\mathbf{R}_\mathbf{H}\boldsymbol{\xi}^H)\right)\circ\mathbf{G}^H\right]_{:,n}\right| - [\boldsymbol{\mathcal{R}}_{\mathbf{h}_\mathcal{P}}]_{\mathcal{P}_i,\mathcal{P}_i}\right).\end{aligned} \tag{16}$$

Further, the IR extrapolation factor can be calculated as

$$f : \{\mathbf{R}_{\boldsymbol{\mathcal{H}},\mathbf{h}_\mathcal{P}}\left(\bar{\mathbf{R}}_{\mathbf{h}_\mathcal{P}}\right)^{-1}, L^2K^2 \times |\mathcal{P}|\} \rightarrow f : \{\boldsymbol{\Lambda}, LK \times LK \times |\mathcal{P}|\}. \tag{17}$$

Finally, replacing $y_{\mathcal{P}_i}$ in Eq. (7) with $\bar{y}_{\mathcal{P}_i}$, we can estimate channel using Eq. (9). Generally, the estimation accuracy of IR extrapolation is higher than that of NIR extrapolation. The reason is that the statistical properties of the interference are no longer considered.

TABLE I
SIMULATION PARAMETERS

	Parameter name	Value
Shared	Number of subcarriers	$L = 24$
	Subcarrier spacing	$F = 15$ kHz
	Sampling rate	$f_s = 5FL$ Hz
	Number of pilots	$\lvert\mathcal{P}\rvert = 16$
	MIR-($\mathbf{H}$) measured environment	Indoor, 560km/h
	Constellation	64-QAM
OFDM	Number of symbols	$K = 14$
	CP length	4.76μs
FBMC	Number of symbols	$K = 30$
	Prototype filter, Overlap factor	PHYDYAS, 4
	Number of guard symbols	$\lvert\mathcal{G}\rvert = 64$

IV. NUMERICAL RESULTS

To verify the usability of MIR-($\mathbf{H}$), we perform a series of experiments. Unless otherwise noted, the simulation parameters are summarized in Table I. Note that in FBMC, each pilot symbol is equipped with 4 guard symbols to mitigate inherent interference. In the time-frequency resource $K_\mathrm{ofdm}T \approx K_\mathrm{fbmc}\frac{T}{2} = 1$ms and $FL = 360$kHz, the overheads of OFDM and FBMC are $\frac{FLT_{CP}K_\mathrm{ofdm}+TF|\mathcal{P}|}{K_\mathrm{ofdm}TLF} \approx 11.4\%$ and

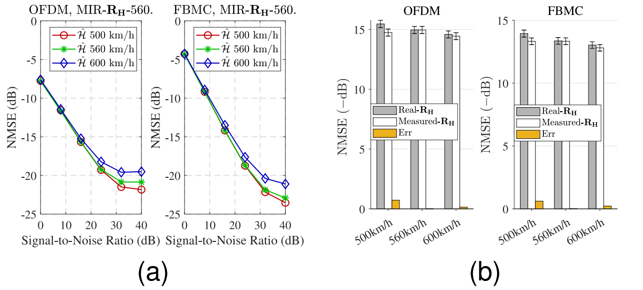

Fig. 1. (a) Estimation accuracy of the 560km/h measured $\mathbf{R_H}$ for the [500, 560, 600] km/h channels. (b) Estimation accuracy of actual $\mathbf{R_H}$, MIR-$\mathbf{R_H}$-560 and deviation.

$\frac{TF(|\mathcal{P}|+|\mathcal{G}|)/2}{K_{\text{fbmc}}TLF/2} = 11.1\%$, respectively. Thus, we ensure that both have the same resource overhead.

A. Error Analysis

Our channel estimation scheme relies on the correlation matrix of MIR-($\mathbf{H}$). Often, measured values cannot accurately describe the actual case, which leads to estimation error. To verify the usability of the measured values, we estimate the channel with [500, 560, 600] km/h using the measured value with mobility of 560 km/h and calculate the estimation error. To simulate the real channel, we adopt the "Extended Vehicular A (EVA)" model provided by 3GPP. We use the Normalized Mean Square Error (NMSE) as an evaluation criterion for accuracy, denoted as

$$\bar{e}^2 = 10\lg\left(||\hat{\boldsymbol{\mathcal{H}}} - \boldsymbol{\mathcal{H}}||_{m1}^2/||\boldsymbol{\mathcal{H}}||_{m1}^2\right). \quad (18)$$

Here, $\|\cdot\|_{m1}$ represents the $m1$-norm of the matrix. Fig. 1(a) shows the estimation accuracy of [500, 560, 600] km/h channels for 560 km/h measured values. Note that we currently only consider NIR extrapolation. We observe that for a velocity deviation of 50km/h, the error of the estimation accuracy does not exceed 3dB. This indicates that the measured value describes the real value with a tolerance of 7%–12%. Additionally, Fig. 1(a) also reflects the channel estimation accuracy in different Doppler spreads (i.e., different mobility). In the same SNR, the higher the mobility, the lower the estimation accuracy. Further, we assess the deviation between the estimated accuracy of the actual $\mathbf{R_H}$ (calculated by EVA) and MIR-$\mathbf{R_H}$-560. We similarly consider channels of [500, 560, 600] km/h with SNR of 15dB. Fig. 1(b) shows the estimated accuracy and deviation for actual $\mathbf{R_H}$ versus MIR-$\mathbf{R_H}$-560. We observe that the estimated accuracy of the measured values deviates less than 1dB from the actual values. This proves that we can select the corresponding MIR-($\mathbf{H}$) estimate channel according to the practical use cases.

B. NMSE Performance

Considering the problem of practical deviations, we perform subsequent experiments using a 500 km/h EVA channel. The higher the pilot power, the more accurate the channel estimation. Thus, the pilot-data power offset ρ has an impact on the estimation accuracy. Fig. 2(a) shows the influence of ρ on NMSE. Note that we consider both NIR and IR extrapolations.

Further, to evaluate the channel estimation accuracy of our scheme in different delay spreads, we adopt the 3GPP

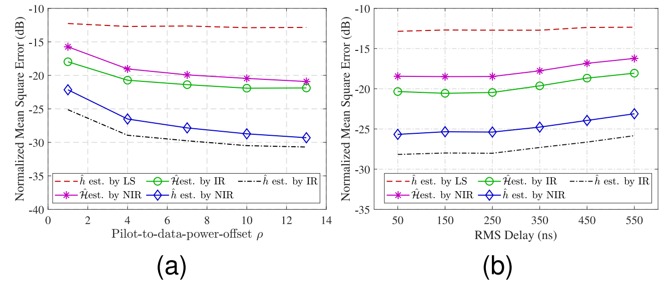

Fig. 2. (a) Influence of the pilot-data power offset ρ and (b) Delay spreads on the estimation accuracy with SNR = 25dB.

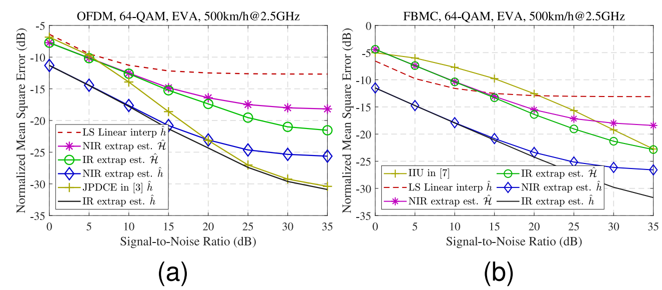

Fig. 3. (a) NMSE performance of OFDM. (b) NMSE performance of FBMC.

"TDL-A" channel model with variable Root Mean Square (RMS) delay spread. Fig. 2(b) shows the channel estimation accuracy of our scheme in different delay spreads. The estimation accuracy decreases with increasing RMS delay spread due to delayed spread mismatch. However, the tolerance does not exceed 5dB. Thus, the MIR-$\mathbf{R_H}$-560 is still available. To balance the practical application with the estimation accuracy, we set ρ to 2. In FBMC, the power of the guard symbols is 0. Thus, we can raise ρ to 4. Fig. 3(a) and Fig. 3(b) show the NMSE performance for OFDM and FBMC channel estimation, respectively. Note that the existing methods cannot be compared in both FBMC and OFDM simultaneously due to incompatibility. In OFDM, Joint Pilot Design Channel Estimation (JDPCE) [3] is compared, while in FBMC, Intrinsic Interference Utilization (IIU) [7] is compared. We can observe that the estimation accuracy of LS linear interpolation is extremely low. The reason is that linear extrapolation cannot accurately characterize the time-varying properties. On the other hand, $\boldsymbol{\mathcal{H}}$ contains both channel-induced and inherent interference. From Fig. 3, we can see that the estimation accuracy of $\boldsymbol{\mathcal{H}}$ is lower than that of $\mathbf{h}$. The reason is that the estimation of $\boldsymbol{\mathcal{H}}$ also includes the prediction of interference, which is extremely difficult. Fig. 3 also supports another conclusion: estimation accuracy suffers from a saturation effect. That is, the interference cannot be completely eliminated, resulting in the estimation accuracy no longer improving with increasing SNR.

C. Complexity Analysis

The computational requirements of the MIR-($\mathbf{H}$)-based channel estimation contain two main parts: obtaining the extrapolation matrix and extrapolation. According to Eq. (10), the complexity of obtaining the extrapolation matrix is $O(|\mathcal{P}|^3 + L^2K^2|\mathcal{P}|^2)$. However, Once the extrapolation matrix

TABLE II
COMPLEXITY COMPARISON

JDPCE in [3]	$\gg O\left(L^3K^3\lvert\mathcal{P}\rvert^3+\lvert\mathcal{P}\rvert\right)$
IIU in [7]	$O\left(4\lvert\mathcal{P}\rvert L^2(K+1)^2-K+5\right)$
BEM receiver in [12]	$O\left(\mathcal{I}\left(2Q^3D^3+\lvert\mathcal{P}\rvert L^3K^3\right)\right)$
MIR-($\mathbf{H}$)-based scheme	$O\left(\lvert\mathcal{P}\rvert^3+L^2K^2\lvert\mathcal{P}\rvert^2\right)+O\left(\lvert\mathcal{P}\rvert L^2K^2\right)$

is obtained, its calculation no longer affects the total complexity. According to Eq. (9), the complexity of extrapolation is $O(|\mathcal{P}|L^2K^2)$. The complexity comparison of our scheme with existing JDPCE [3], IIU [7] and BEM receiver [12] is shown in Table II.

Note that the complexity of JDPCE is induced by deep neural networks and is difficult to accurately characterize. Thus, Table II provides only the computational requirements for preprocessing. In Table II, $\mathcal{I}$, Q and D denote the number of iterations, BEM order and atomic dimension, respectively.

V. CONCLUSION

In this letter, we proposed a channel estimation scheme for OFDM, FBMC and other arbitrary linear modulations. The proposed MIR-($\mathbf{H}$)-based estimation scheme can be applied to doubly selective channel with high estimation accuracy. Particularly, IR extrapolation based on interference removal can further improve the channel estimation performance. To obtain practical applications in OFDM and FBMC, we analyze the estimated accuracy and deviation of the measured and actual values. The provided experimental data proves the usability of the measured values. It is worth noting that the proposed scheme is also applicable to flat fading channels.

APPENDIX
PROOF OF LEMMA 1

We extend the orthogonal projection theorem in [16] to $\boldsymbol{\mathcal{H}}$ (with minor modification) and consider MIR-($\mathbf{H}$) available. Then

$$\begin{aligned}
&\mathbb{E}\left\{\left(\boldsymbol{\mathcal{H}}-\hat{\boldsymbol{\mathcal{H}}}\right)\hat{\boldsymbol{\mathcal{H}}}^H\right\}=\mathbb{E}\{\boldsymbol{\mathcal{H}}\hat{\boldsymbol{\mathcal{H}}}^H-\hat{\boldsymbol{\mathcal{H}}}\hat{\boldsymbol{\mathcal{H}}}^H\}\\
&=\mathbb{E}\left\{\mathbf{G}^H\mathbf{H}\mathbf{G}\sum\nolimits_{i=1}^{|\mathcal{P}|}\hat{\mathbf{h}}_{\mathcal{P}_i}^H\bar{\boldsymbol{\Lambda}}_i^H-\sum\nolimits_{i=1}^{|\mathcal{P}|}\bar{\boldsymbol{\Lambda}}_i\hat{\mathbf{h}}_{\mathcal{P}_i}\hat{\mathbf{h}}_{\mathcal{P}_i}^H\bar{\boldsymbol{\Lambda}}_i^H\right\}\\
&=\mathbb{E}\left\{\sum_{i=1}^{|\mathcal{P}|}\left(\left(\mathbf{G}^T\otimes\mathbf{G}^H\right)\mathrm{vec}\{\mathbf{H}\}\hat{\mathbf{h}}_{\mathcal{P}_i}^H-\bar{\boldsymbol{\Lambda}}_i\hat{\mathbf{h}}_{\mathcal{P}_i}\hat{\mathbf{h}}_{\mathcal{P}_i}^H\right)\bar{\boldsymbol{\Lambda}}_i^H\right\}\\
&=\sum_{i=1}^{|\mathcal{P}|}\left(\mathbb{E}\left\{\left(\mathbf{G}^T\otimes\mathbf{G}^H\right)\mathrm{vec}\{\mathbf{H}\}\hat{\mathbf{h}}_{\mathcal{P}_i}^H\right\}-\bar{\boldsymbol{\Lambda}}_i\mathbb{E}\left\{\hat{\mathbf{h}}_{\mathcal{P}_i}\hat{\mathbf{h}}_{\mathcal{P}_i}^H\right\}\right)\bar{\boldsymbol{\Lambda}}_i^H\\
&=\mathbf{0}.
\end{aligned}\tag{19}$$

Due to $\bar{\boldsymbol{\Lambda}}_i^H\neq 0$ and we consider $\hat{\mathbf{h}}_{\mathcal{P}_i}=\mathbf{h}_{\mathcal{P}_i}=(\mathbf{g}_{\mathcal{P}_i}^T\otimes\mathbf{g}_{\mathcal{P}_i}^H)\mathrm{vec}\{\mathbf{H}\}$ to be determined by MIR-($\mathbf{H}$), thereby

$$\begin{aligned}
&\mathbb{E}\left\{\left(\mathbf{G}\otimes\mathbf{G}^H\right)\mathrm{vec}\{\mathbf{H}\}\mathbf{h}_{\mathcal{P}_i}^H\right\}-\bar{\boldsymbol{\Lambda}}_i\mathbb{E}\left\{\mathbf{h}_{\mathcal{P}_i}\mathbf{h}_{\mathcal{P}_i}^H\right\}\\
&=\mathbb{E}\left\{\left(\mathbf{G}\otimes\mathbf{G}^H\right)\mathrm{vec}\{\mathbf{H}\}\mathrm{vec}\{\mathbf{H}\}^H\left(\mathbf{g}_{\mathcal{P}_i}^T\otimes\mathbf{g}_{\mathcal{P}_i}^H\right)^H\right\}\\
&-\bar{\boldsymbol{\Lambda}}_i\mathbb{E}\left\{\mathbf{h}_{\mathcal{P}_i}\mathbf{h}_{\mathcal{P}_i}^H\right\}\\
&=\mathbf{R}_{\boldsymbol{\mathcal{H}},\mathbf{h}_{\mathcal{P}_i}}-\bar{\boldsymbol{\Lambda}}_i\mathbf{R}_{\mathbf{h}_{\mathcal{P}_i}}=\mathbf{0}.
\end{aligned}\tag{20}$$

According to Eq. (20), $\bar{\boldsymbol{\Lambda}}_i\in\mathbb{C}^{L^2K^2\times|\mathcal{P}_i|}$ can be calculated as

$$\bar{\boldsymbol{\Lambda}}_i=\mathbf{R}_{\boldsymbol{\mathcal{H}},\mathbf{h}_{\mathcal{P}_i}}\left(\mathbf{R}_{\mathbf{h}_{\mathcal{P}_i}}\right)^{-1}.\tag{21}$$

Considering all pilot positions, we can calculate $\boldsymbol{\Lambda}\in\mathbb{C}^{L^2K^2\times|\mathcal{P}|}$ as

$$\boldsymbol{\Lambda}=\mathbf{R}_{\boldsymbol{\mathcal{H}},\mathbf{h}_{\mathcal{P}}}\left(\mathbf{R}_{\mathbf{h}_{\mathcal{P}}}\right)^{-1}.\tag{22}$$

REFERENCES

[1] P. Singh, H. B. Mishra, A. K. Jagannatham, K. Vasudevan, and L. Hanzo, “Uplink sum-rate and power scaling laws for multi-user massive MIMO-FBMC systems,” *IEEE Trans. Commun.*, vol. 68, no. 1, pp. 161–176, Jan. 2020.

[2] Y. Wang, Q. Guo, J. Xiang, L. Wang, and Y. Liu, “Bi-orthogonality recovery and MIMO transmission for FBMC systems based on non-sinusoidal orthogonal transformation,” *Signal Process.*, vol. 219, Jun, 2024, Art. no. 10942.

[3] H. Fu, W. Si, and I.-M. Kim, “Deep learning-based joint pilot design and channel estimation for OFDM systems,” *IEEE Trans. Commun.*, vol. 71, no. 8, pp. 4577–4590, Aug. 2023.

[4] P. Cheng et al., “Channel estimation for OFDM systems over doubly selective channels: A distributed compressive sensing based approach,” *IEEE Trans. Commun.*, vol. 61, no. 10, pp. 4173–4185, Oct. 2013.

[5] D. Ren, J. Li, G. Lu, and J. Ge, “Joint channel estimation and equalization using new AFB output signal models for FBMC/OQAM systems,” *IEEE Trans. Commun.*, vol. 69, no. 6, pp. 4186–4201, Jun. 2021.

[6] D. Ren, J. Li, G. Zhang, G. Lu, and J. Ge, “Multi-tap channel estimation for preamble-based FBMC/OQAM systems,” *IEEE Access*, vol. 8, pp. 176232–176240, 2020.

[7] D. Chen, R. Wang, and T. Jiang, “Channel estimation and pilot symbol optimization based on intrinsic interference utilization for OQAM/FBMC systems,” *IEEE Trans. Signal Process.*, vol. 69, pp. 4595–4606, Aug. 2021.

[8] D. Kong, J. Li, K. Luo, and T. Jiang, “Reducing pilot overhead: Channel estimation with symbol repetition in MIMO-FBMC systems,” *IEEE Trans. Commun.*, vol. 68, no. 12, pp. 7634–7646, Dec. 2020.

[9] D. Kong, X. Zheng, Y. Zhang, and T. Jiang, “Frame repetition: A solution to imaginary interference cancellation in FBMC/OQAM systems,” *IEEE Trans. Signal Process.*, vol. 68, pp. 1259–1273, Feb. 2020.

[10] W. Liu, S. Schwarz, M. Rupp, D. Chen, and T. Jiang, “Preamble-based channel estimation for OQAM/FBMC systems with delay diversity,” *IEEE Trans. Wireless Commun.*, vol. 19, no. 11, pp. 7169–7180, Nov. 2020.

[11] Q. Guo, Y. Wang, J. Xiang, and Y. Zhong, “Complex Gaussian ratio-based bit error probability calculation for PAM-FBMC systems,” *IEEE Commun. Lett.*, vol. 28, no. 4, pp. 788–792, Apr. 2024.

[12] Y. Wang, Q. Guo, J. Xiang, and Y. Liu, “Doubly selective channel estimation and equalization based on ICI/ISI mitigation for OQAM-FBMC systems,” *Phys. Commun.*, vol. 59, Aug. 2023, Art. no. 102120.

[13] I. Barhumi, G. Leus, and M. Moonen, “Optimal training design for MIMO OFDM systems in mobile wireless channels,” *IEEE Trans. Signal Process.*, vol. 51, no. 6, pp. 1615–1624, Jun. 2003.

[14] A. Y. Panah, R. G. Vaughan, and R. W. Heath, “Optimizing pilot locations using feedback in OFDM systems,” *IEEE Trans. Veh. Technol.*, vol. 58, no. 6, pp. 2803–2814, Jul. 2009.

[15] R. Nissel, F. Ademaj, and M. Rupp, “Doubly-selective channel estimation in FBMC-OQAM and OFDM systems,” in *Proc. IEEE 88th Veh. Technol. Conf.*, 2018, pp. 1–5.

[16] M. Ekstrom, “Realizable wiener filtering in two dimensions,” *IEEE Trans. Acoust., Speech, Signal Process.*, vol. 30, no. 1, pp. 31–40, Feb. 1982.

[17] S. Caban, J. Rodas, and J. A. García-Naya, “A methodology for repeatable, off-line, closed-loop wireless communication system measurements at very high velocities of up to 560 km/h,” in *Proc. IEEE Int. Instrum. Meas. Technol. Conf.*, 2011, pp. 1–5.

[18] S. Caban, R. Nissel, M. Lerch, and M. Rupp, “Controlled OFDM measurements at extreme velocities,” in *Proc. 6th Extreme Conf. Commun. Comput.*, 2014, pp. 1–6.